Solid State Science and Technology, Vol. 31, No. 2 (2023), 71-81
https://doi.org/10.66514/ssst31-2-71-81

COMPARATIVE STUDY OF SUPERCONDUCTING PROPERTIES FOR $YBa_2Cu_3O_{7-\delta}$ ADDED CA-COMPOUNDS SYNTHESIZED UNDER DIFFERENT ANNEALING CONDITIONS

Siew Hong Yap[1], Mohd Mustafa Awang Kechik [1,], Hussien Baqiah[2], Soo Kien Chen[1], Kean Pah Lim[1], Muhammad Kashfi Shabdin[1], Mohd Hafiz Mohd Zaid[1], Yazid Yaakob[1], Mohd Khalis Abdul Karim[1], Zhi Wei Loh[1], Abdul Halim Shaari[1], Muralidhar Miryala[3]*

[1]Superconductor & Thin Films Laboratory, Department of Physics, Faculty of Science, Universiti Putra Malaysia, 43400 UPM Serdang, Selangor Darul Ehsan, Malaysia

[2]Shandong Key Laboratory of Biophysics, Institute of Biophysics, Dezhou University, No. 566 University Rd. West, Dezhou, Shandong, China

[3]Materials for Energy and Environmental Laboratory, Superconducting Materials Group, Graduate School of Science & Engineering, Shibaura Institute of Technology, 3-7-5 Foxesu, Koto-ku, Tokyo 135-8548, Japan

Received: 1 Dec. 2023; Accepted: 31 Dec. 2023

**Corresponding author; Email: mmak@upm.edu.my*

ABSTRACT

This comparative investigation is focused on producing bulk $YBa_2Cu_3O_{7-\delta}$ (Y-123) through thermal treatment method, employing two distinct annealing conditions: oxygen flow and ambient conditions. This research explored the potential of using chicken eggshells as a source of calcium compounds (CaO, $CaCO_3$ and $Ca(OH)_2$) for Y-123 synthesis, incorporating deficient Ca-compound (CaES) concentrations, such as 0.0100 wt.%. The XRD results showed that the structure of all the samples is orthorhombic. The inclusion of deficient Ca compounds suggested an altered pattern of grain degradation within the Y-123 matrix system, accompanied by the emergence of other non-superconducting phases. The superconducting properties, including electrical resistivity, were examined through electrical resistance measurements. Unexpectedly, the superconducting characteristics improved upon introducing deficient Ca compounds into the Y-123 system, particularly enhancing the rapidity of annealing at ambient conditions. The hole concentration, p increased in the added CaES samples compared to the non-added Y-123. This increase was observed alongside the narrowest superconducting transition width, approximately ΔT_c = 2.95 K and $\Delta T_c^{MF\text{-}zero}$ = 1.46 K, specifically for the added CaES at 0.0100 wt.% annealed in ambient conditions, in contrast to CaES annealed in oxygen flow. Additionally, the residual resistivity (ρ_o) was lowest at 336 μΩcm among all samples. This enhancement improves the superconducting properties, emphasizing the potential for cost savings compared to oxygen flow costs.

Keywords Artificial pinning centers; superconducting transition width; hole concentration; grains degradations

INTRODUCTION

Following the discovery of $YBa_2Cu_3O_{7-\delta}$ (Y-123) high-temperature superconductor, the combination of alkali metals with the Y-123 system, whether through substitution or additions, has garnered significant attention in both research and industrial sectors [1, 2]. The production of superior-quality bulk Y-123 remains a persistent focus in the exploration of various high-temperature superconductors, particularly within the copper-oxide family. Adding a deficient quantity of alkali metal is anticipated to enhance the quality of grain boundaries and the connectivity of grains in Y-123. It also contributes to the formation of fine particles that can serve as pinning centers in the superconductor. Alkali metal oxides have gained significant attention across multiple sectors, as researchers seek novel and efficient approaches to regulate and produce metal oxide nanostructures [3, 4]. Consequently, with previous applications in technology, CaO has been recognized as a crucial foundational material in high-Tc superconductors [5, 6].

Apart from that, various approaches were employed to synthesize high-quality superconductors within the copper-oxide family such as solid-state reaction, co-precipitation, sol-gel, and melt processing [7-11]. Refinement of these methods involved diverse heat treatment processes to enhance superconducting properties. Heat treatment significantly affects weak link behavior in Y-123, which is associated with structural inhomogeneities, pores, voids, and impurity phases at grain boundaries. This refinement aims to enhance both the superconducting transition width (ΔT_c) and critical current density (J_c) by incorporating artificial pinning centers (APCs) into the copper oxide system [12, 13]. Various metallic and non-metallic elements, along with alkali metals [14, 15], were introduced alongside different heat treatment processes like calcination, sintering, and annealing. Significant alterations in microstructure, densification, and crystal growth occur with variations in heat treatment conditions. Annealing, particularly during sintering [16], plays a crucial role. It is widely known that annealing in an oxygen environment notably enhances the superconducting properties of Y-123 superconductors by improving crystal structure and reducing defects [17]. It affects the oxidation state of copper ions, the formation of the Y-123 phase, and the oxygen content of the final product. However, the specifics and uncertainties regarding the superconducting characteristics of the Y-123 system, enriched with APCs and subjected to annealing under ambient conditions, remain unexplored.

In this study, our goal was to use an environmentally friendly method, thermal treatment, to synthesize Y-123 added with Ca-compounds extracted from eggshells (Y-123-CaES). The investigation involved extensive research into the green synthesis of Y-123 added with calcium compounds (CaO, $CaCCO_3$ and $Ca(OH)_2$) by examining the specimens annealed in two conditions: oxygen flow and ambient conditions.

MATERIALS AND METHOD

Specimen Preparation

High-purity metal nitrates (~99%) $Y(NO_3)_2{\cdot}6H_2O$, $Ba(NO_3)_2$, and $Cu(NO_3)_2{\cdot}2.5H_2O$ sourced from Alfa Aesar were mixed with polyvinyl pyrrolidone (PVP), stirred, and dried at 110 °C for 24 h. The resulting green dry gel was powdered, pre-calcinated at 600 °C for 4 h, and calcinated at 910°C in air for 24 h. After grinding, Ca-compounds from chicken eggshells (CaES) [18] were added, and the mixture was re-ground. Finely ground

powders were pressed into pellets, sintered at 980°C for 24 h under two different annealing conditions, namely in oxygen flow and ambient conditions, in a double-tube furnace.

Specimen Investigation

The examination of phase development and crystal structure in the specimens utilized the x-ray diffraction (XRD) method on a PW 3040/60 MPD X'Pert Pro Panalytical Philips DY 1861 X-ray diffractometer, employing a Cu-K radiation source with a wavelength of 1.45 Å. The scanning spanned the 2θ range of 20^o – 80^o, with an incremental step size of 0.03^o. The superconducting properties, specifically electrical resistivity measurements, were also carried out using an in-house homemade setup utilizing the four-point probe technique.

RESULTS AND DISCUSSION

Structural and Phase Formation Analysis

Figure 1 shows the XRD patterns of the pure Y-123 and the addition of deficient concentration of CaES (0.0100 wt.%) into Y-123. All samples resultant a major phase $YBa_2Cu_3O_{7-\delta}$ (Y-123) and other phases such as $YBa_2Cu_3O_5$ (Y-211) and $BaCuO_2$. All the final samples were confirmed to exhibit the formation of the orthorhombic Y-123 phase, *Pmmm* space group (ICSD: 98-006-0398), with prominent intensity peaks for Y-123 found at $2\theta \approx 32.5^o$ and $2\theta \approx 32.8^o$, corresponding to Miller indices (013) and (103), respectively. The orthorhombic crystal structure was also evident in the peaks for other phases such as Y-211 (ICSD: 98-002-5960) and BaCuO2 (ICSD: 98-002-5029). This discovery aligns with previous research [8, 19, 20]. Detailed observations of the orthorhombicity value and phases present in the specimens are provided in Table 1 and 2, respectively. No secondary phases related to Ca-compounds were identified in both Y-123-CaES 0.0100 wt.% samples annealed under oxygen flow and ambient conditions. This suggests that the deficient addition of CaES compounds, such as CaO, $Ca(OH)_2$ and $CaCO_3$, did not react with the Y-123 host matrix to form other Ca-based compounds [21]. Instead, it may have generated unit cell defects while maintaining a stable Y-123 matrix system [22].

The lattice parameters (*a*, *b*, and *c*) and oxygen content ($O_{7-\delta}$), as well as information on unit cell volume, volume fractions, crystallite size, and lattice strains of Y-123, were determined through Rietveld refinement method using HighScore Plus software, as presented in Tables 1 and 2, respectively. Table 1 shows that all samples exhibit an orthorhombic crystal structure. The lattice parameters of Y-123 show slight changes after the addition of a deficient concentration of CaES, supporting the idea that Ca-compounds did not directly substitute into the Y-123 matrix system [23] but entered the inter-grain regions. The highest orthorhombicity value, 0.00878, was observed at a deficient CaES concentration of 0.0100 wt.% annealed under ambient conditions, with an optimal oxygen content of 6.8281, calculated using equation ($7-\delta = 75.25 - 5.86c$), where c represents the lattice parameter on the y-axis in the Y-123 matrix system [21, 24]. This indicates that thinning twin borders correlates with heightened oxygen ordering along the *b*-axis in the Cu-O-Cu chain and augmentation in twin density [25]. Table 2 indicates that Y-123 volume fractions in specimens with deficient CaES exceed those in pure Y-123.

Additionally, the deficient concentration of CaES at 0.0100 wt.% annealed under ambient conditions exhibits the lowest lattice strain (0.183 %) and the highest crystallite size (998 Å). This results in the presence of non-superconducting phases like Y-211 and $BaCuO_2$ at grain boundaries, facilitated by the gradual oxygen capture, creating an ideal environment for forming a stoichiometric oxide compound. This process may influence the grain boundary structure, leading to the induction of superconducting properties [26].

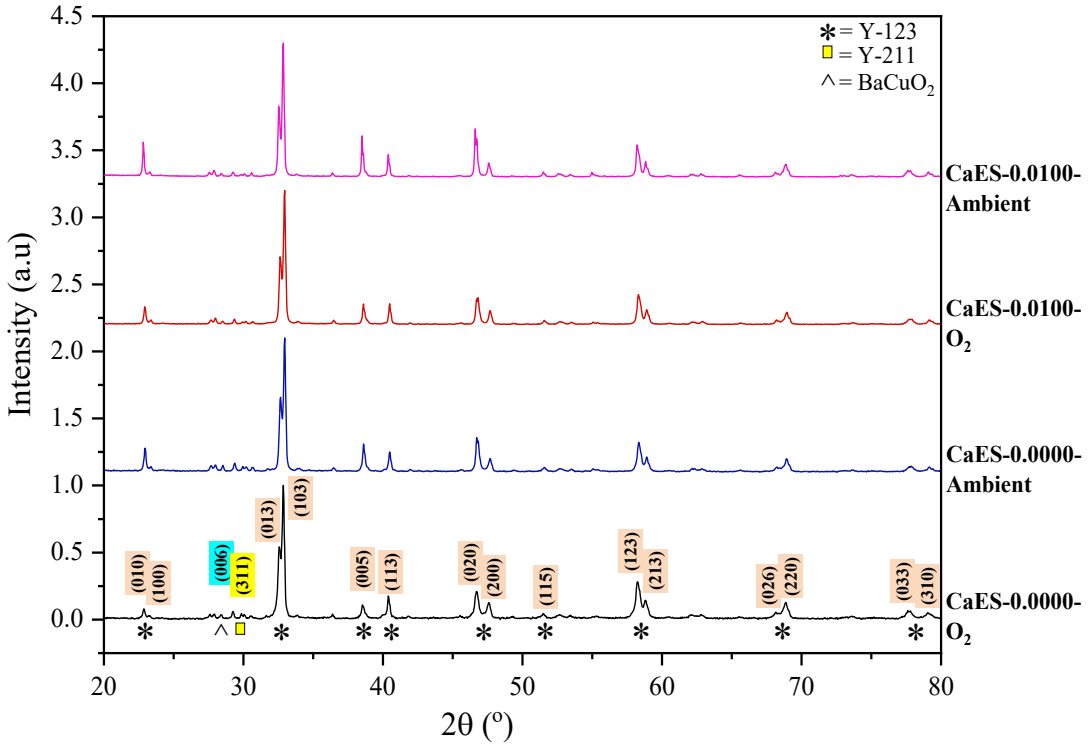

Figure 1. XRD pattern of pure Y-123 (CaES-0.0000-O_2 annealed in oxygen flow and CaES-0.0000-ambient annealed in ambient conditions) and Y-123-CaES 0.0100 wt.% (CaES-0.0100-O_2 annealed in oxygen flow and CaES-0.0100-ambient annealed in ambient conditions)

Table 1. The lattice parameters, orthorhombicity and oxygen content for pure Y-123 and Y-123-CaES 0.0100 wt.% at two different annealing conditions

Specimens (wt.%)	Lattice Parameters (Å)			Orthorhombicity |(b-a)/(a+b)|	δ	$O_{7-\delta}$
	a-axis	b-axis	c-axis			
CaES-0.0000-O_2	3.8231(3)	3.8858(4)	11.6818(16)	0.00813	0.2053	6.7947
CaES-0.0000-Ambient	3.8237(3)	3.8882(4)	11.6870(15)	0.00836	0.2358	6.7642
CaES-0.0100-O_2	3.8214(2)	3.8865(3)	11.6851(9)	0.00845	0.2247	6.7753
CaES-0.0100-Ambient	3.8193(3)	3.8870(5)	11.6761(17)	0.00878	0.2440	6.8281

Table 2. The volume fractions, volume of unit cell Y-123, crystallite size and lattice strain for pure Y-123 and Y-123-CaES 0.0100 wt.% at two different annealing conditions

Specimens (wt.%)	Volume Fraction			Volume of Unit Cell Y-123 ($Å^3$)	Crystallite Size Y-123 (Å)	Lattice Strain Y-123 %
	Y-123 (%)	Y-211 (%)	$BaCuO_2$ (%)			
CaES-0.0000-O_2	89.1	3.4	7.5	173.5424	563	0.282
CaES-0.0000-Ambient	88.5	3.4	8.0	173.7514	767	0.221
CaES-0.0100-O_2	94.8	1.7	3.6	173.5444	828	0.209
CaES-0.0100-Ambient	93.7	2.4	3.9	173.3389	998	0.183

Microstructural and Elemental Analysis

The average grain size was determined by analyzing 200 randomly selected grains using Image-*J* software. Figure 2 presents FESEM images and grain size distribution histograms for all specimens. These specimens exhibit irregularly shaped and randomly distributed grains, ranging in size from approximately 1 to 2 μm with the presence of pores or void defects. Referring to Table 3, it is evident that Y-123-CaES at 0.0100 wt.% exhibited a lower average grain size compared to pure Y-123 specimens under both annealing conditions. The surface morphology images depict an alteration in grain refinement initiated by the breakdown of some larger grains into smaller ones after the addition of CaES. In Fig. 2, the grain size distribution histogram makes it clear that the grain distribution for 0.0100 wt.% CaES annealed under ambient conditions displays the most uniform curve. Therefore, annealing with a deficient concentration of CaES in ambient conditions may facilitate improved grain alignment with fewer pores, thus enhancing superconductivity, i.e., J_c [7], compared to CaES annealed in oxygen flow.

Table 3. Average grain sizes for pure Y-123 and Y-123-CaES 0.0100 wt.% annealed at two different annealing conditions

Specimens (wt.%)	Average Grain Sizes (μm)
CaES-0.0000-O_2	1.35 (±0.54)
CaES-0.0000-Ambient	1.99 (±0.53)
CaES-0.0100-O_2	1.25 (±0.50)
CaES-0.0100-Ambient	1.55 (±0.59)

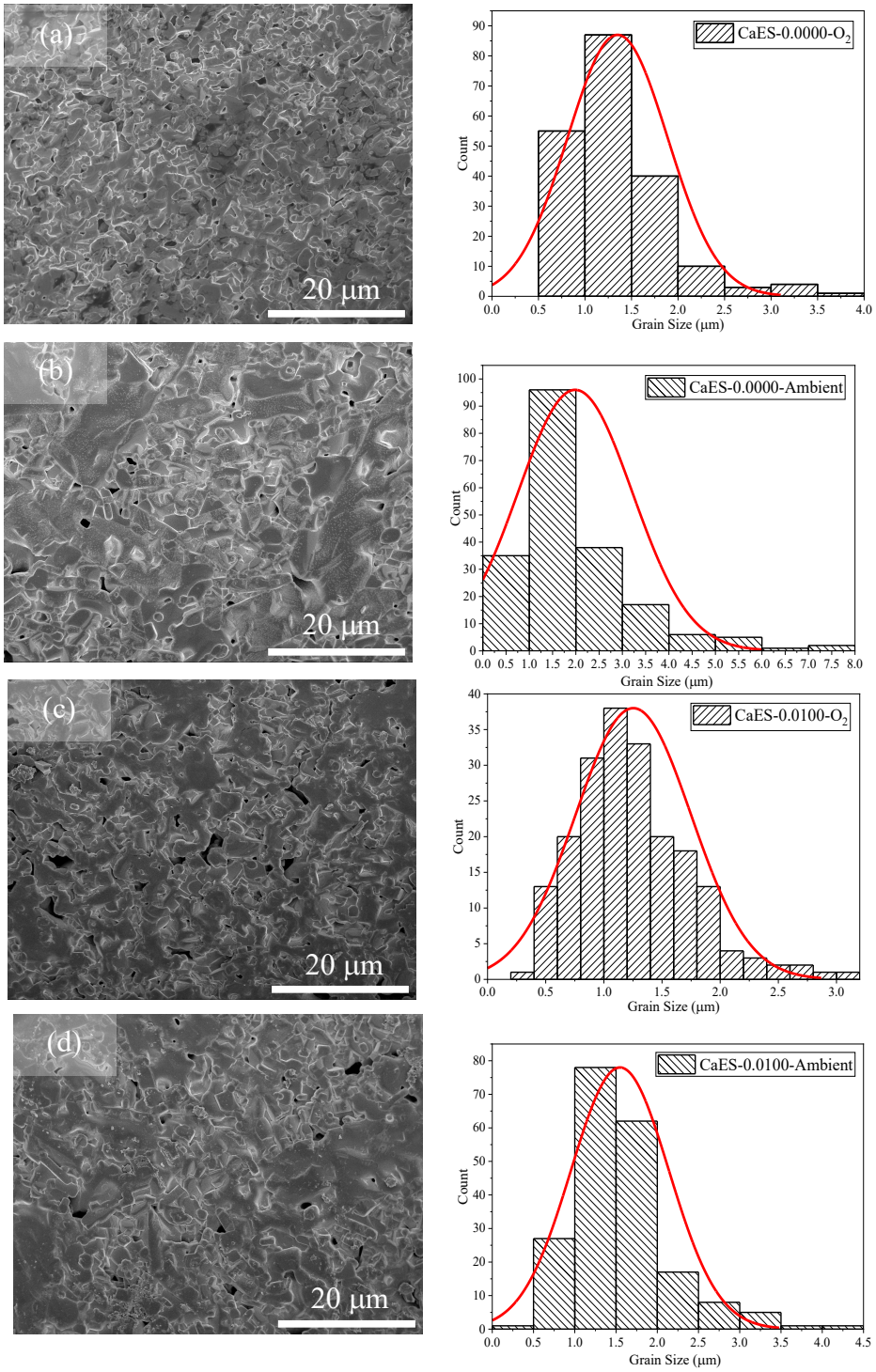

Figure 2. FESEM surface micrographs and grain size distribution histogram for (a) pure Y-123 annealed in oxygen flow, (b) pure Y-123 annealed under ambient, (c) Y-123-CaES 0.0100 wt.% annealed in oxygen flow and (d) Y-123-CaES 0.0100 wt.% annealed under ambient

Electrical Resistivity Analysis

The temperature-dependent resistivity of the Y-123 superconductor was assessed using a standard DC four-point probe, following Ohm's Law equation: $V=IR$, where V represents the voltage across the two inner probes, I is the applied current through the two outer probes, and R is the resistance. The evaluation of electrical resistivity (ρ) against temperature (T) for CaES addition is depicted in Fig. 3, with their corresponding derivatives shown in Fig. 4. In Fig. 3, specimens with deficient concentrations of CaES exhibit metallic behavior in the normal state above the onset critical transition temperature ($T_{c\text{-onset}}$). The values of $T_{c\text{-onset}}$ are notably higher with the inclusion of CaES compared to pure Y-123, indicating the influence of CaES addition on the samples' normal and superconducting states [27]. Referring to Fig. 3 and 4, all samples exhibit a single-step transition, except for pure Y-123 annealed under oxygen flow, which almost shows a double transition characteristic. The single-step transition is associated with the highest orthorhombicity (Table 1) and a significant composition of the Y-123 phase (Table 2) [20]. This characteristic reflects good grain connectivity and the dominance of the Y-123 phase in the samples, contributing to a single-step transition [9, 28]. The transition becomes more evident when analyzing $d\rho/dT$, as illustrated in Fig. 4 (a) and (b). This examination, derived from the resistivity data, demonstrates a systematic decrease in mean field transition temperature, T_c^{MF}, as outlined in Table 4. This decrease signifies the occurrence of the superconducting transition within the grains.

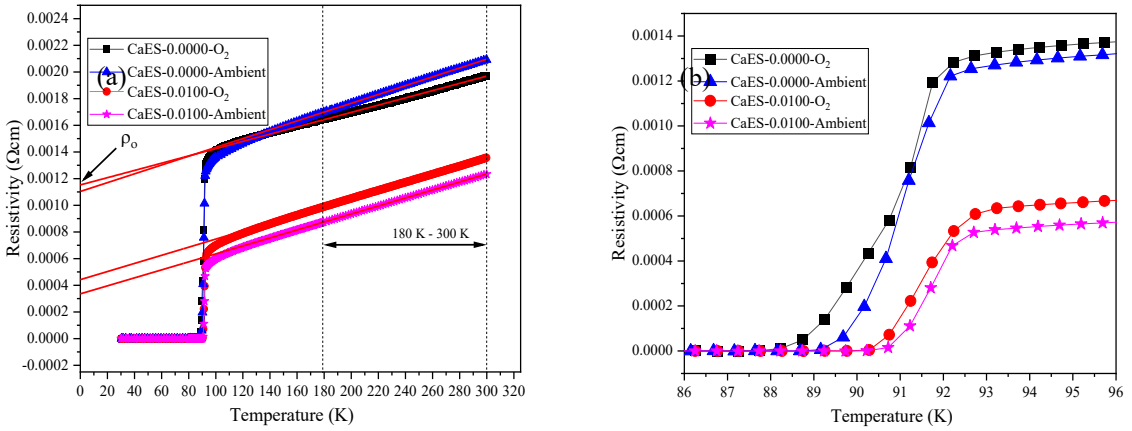

Figure 3. (a) Plot of resistivity, $\rho(T)$, against the temperature range of 30 to 300 K, and (b) a close-up view of the temperature ranges from 86 K to 96 K for pure Y-123 and Y-123-CaES 0.0100 wt.% at two different annealing conditions i.e. oxygen flow and ambient

Table 4 presents the critical parameters tabulated from the analysis of Fig. 3 and 4. The values of $T_{c\text{-onset}}$ and $T_{c\text{-zero}}$ significantly increased with the addition of a deficient concentration of CaES. However, the width of the transition temperatures ΔT_c, decreased at the deficient concentrations of CaES, particularly at 0.0100 wt.%, and reached its lowest point for CaES annealed in ambient conditions at 2.95 K. This implies that the deficient concentration of CaES, introduced at a slow rate of oxygen, causes Ca-compounds to replace oxygen and induce superconductivity at the inter-grains,

demonstrating the smallest ΔT and $\Delta T_c^{MF\text{-}zero}$, suggests an enhancement of superconducting properties.

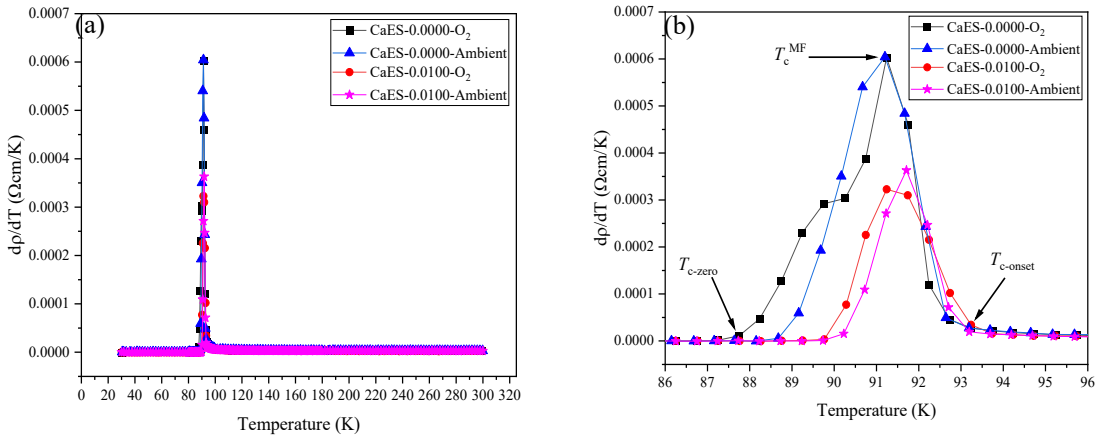

Figure 4. Analysis of the derivative resistivity (a) in the temperature range of 30 to 300 K, and (b) a close-up examination within the range of 86 to 96 K for pure Y-123 and Y-123-CaES 0.0100 wt.% at two different annealing conditions i.e. oxygen flow and ambient

Another aspect of the resistivity analysis is highlighted through the plot of $\rho(T)$ reveals two distinct regions: a non-linear behavior indicative of the superconducting regime and a linear normal state metallic-like behavior, as explained by the Anderson and Zou relationship, $\rho_n(T) = \rho_o + (d\rho/dT)T$. Here, $\rho_n(T)$ represents the normal state resistivity, $d\rho/dT$ is the calculated slope obtained through linear fitting of resistivity in the temperature range from 180 K to 300 K, and ρ_o is the extrapolation of the linear fitting to 0 K. ρ_o serves as the residual temperature and serves as an indicator of specimen homogeneity, impurity, and defect densities within the specimen.

Furthermore, the fluctuation in $T_{c\text{-}zero}$ arises from the changing hole carrier concentration (p) in the CuO_2 planes per CuO ion [29, 30], or the number of holes per Cu. This relationship can be inferred from the parabolic correlation as follows [9, 31]:

$$p = 0.16 - \left[\left(1 - \frac{T_{c-offset}}{T_{c-offset}^{max}}\right)/82.6\right]^{0.5} \quad (1)$$

Another crucial superconducting parameter, the temperature-dependent intrinsic term deriving from electron-electron scattering and the diffusion of elementary excitations, is the slope of resistivity, $d\rho/dT$. Displayed in Table 4, ρ_o (336 μΩcm) and $d\rho/dT$ (2.9967 K) attain their minimum values with the addition of deficient CaES annealed in ambient conditions. This can be ascribed to minimized disorder, reduced inhomogeneities, defects, the lowest occurrence of electron-electron scattering, and the diffusion of elementary excitations in CaES annealed in ambient. Additionally, the decrease in ρ_o implies an increase in the concentration of charge carriers, p, in the cuprate, as demonstrated in Table 4, leading to a decrease in $T_{c\text{-}zero}$. The p for added CaES exhibits an increased value compared to pure Y-123, aligning with the FESEM findings.

Table 4. The superconducting parameters of pure Y-123 and Y-123-CaES annealed at two different annealing conditions

Specimen	$T_{c\text{-onset}}$ (K)	$T_{c\text{-zero}}$ (K)	ΔT_c (K)	T_c^{MF} (K)	$\Delta T_c^{MF\text{-}zero}$ (K)	ρ_o (μΩcm)	$d\rho/dT$ (μΩcm/K)	Hole Concentration (p) -
CaES-0.0000 - O_2	92.73	88.22	4.51	91.24	3.02	1150	2.7206	0.1487
CaES-0.0000 - Ambient	92.64	89.08	3.56	91.20	2.12	1100	3.3065	0.1513
CaES-0.0100-O_2	93.24	89.99	3.25	91.24	1.25	442	3.0434	0.1600
CaES-0.0100-Ambient	93.20	90.25	2.95	91.71	1.46	336	2.9967	0.1584

CONCLUSION

In summary, superior enhancements to the Y-123 system were achieved by adding deficient concentrations of CaES (0.0100 wt.%) using thermal treatment under ambient conditions. XRD analysis revealed good orthorhombic crystal structures, and superconducting properties improved with the addition of Ca-compounds, resulting in smaller average grain sizes. The hole concentration (p) increased in CaES samples, particularly at 0.0100 wt.% annealed in ambient conditions, showing the narrowest superconducting transition width ΔT_c = 2.95 K and $\Delta T_c^{MF\text{-}zero}$ = 1.46 K. Residual resistivity (ρ_o) reached its lowest value at 336 μΩcm. This discovery highlighted the benefits of deficient Ca-compound concentrations for improved grain degradation and surface morphology without affecting average grain size but enhancing oxygen ordering. The homogeneous distribution of Y-211 and $BaCuO_2$ played a crucial role in flux pinning and inter-granular coupling, leading to higher p and stronger Josephson junctions. This highlights the importance of incorporating recycled alkali metal compounds (CaES) from household waste (extracted from chicken eggshells) into the Y-123 matrix system. Specifically, utilizing a deficient concentration of Ca-compounds enhances the superconducting properties. This approach not only offers cost savings compared to oxygen flow methods but also aligns with environmentally friendly practices through a green approach using the thermal treatment method.

ACKNOWLEDGEMENTS

Authors gratefully acknowledge financial support from the Ministry of Higher Education Malaysia (MOHE) for Fundamental Research Grant Scheme FRGS/1/2019/STG02/UPM/02/3 (5540282) Universiti Putra Malaysia. The paper was partly supported by Japan Science and Technology (JST) for the advanced Project Based Learning (aPBL), Shibaura Institute of Technology (SIT) under the Top Global University Project designed by the Ministry of Education, Culture, Sports, and Science & Technology, Japan.

CONFLICT OF INTEREST

The authors declare that they have no known competing financial interests or personal relationships that could have appeared to influence the work reported in this paper.

REFERENCES

[1] B. Khoshnevisan, M. Mohammadi (2016), *Physica C: Superconductivity and its Applications* **523**, 5.

[2] A. Norazidah, H. Azhan, K. Azman, H. Hidayah, J. Hawa (2012), *Advanced Materials Research* **501**, 294.

[3] R. Al-Gaashani, S. Radiman, N. Tabet, A.R. Daud (2011), *Materials Chemistry and Physics* **125**, 846.

[4] E. Comini, C. Baratto, G. Faglia, M. Ferroni, A. Vomiero, G. Sberveglieri (2009), *Progress in Materials Science* **54**, 1.

[5] G. Malandrino, A. Frassica, G.G. Condorelli, G. Lanza, I.L. Fragalà (1997), *Journal of Alloys and Compounds* **251**, 314.

[6] T. Jarlborg (2007), *Physica C: Superconductivity* 454, 5.

[7] E. Hannachi, Y. Slimani, F.B. Azzouz, A. Ekicibil (2018), *Ceramics International* **44**, 18836.

[8] A.N. Kamarudin, M.M. Awang Kechik, M. Miryala, S. Pinmangkorn, M. Murakami, S.K. Chen, H. Baqiah, A. Ramli, K.P. Lim, A.H. Shaari (2021), *Coatings* **11**, 377.

[9] N.M. Hapipi, S.K. Chen, A.H. Shaari, M.M.A. Kechik, K.B. Tan, K.P. Lim (2018), *Journal of Materials Science: Materials in Electronics* 29, 18684.

[10] M.M. Dihom, A.H. Shaari, H. Baqiah, N.M. Al-Hada, Z.A. Talib, C.S. Kien, R.S. Azis, M.M.A. Kechik, L.K. Pah, R. Abd-Shukor (2017), *Ceramics International* **43**, 11339.

[11] M.M. Awang Kechik (2011) Improvement of critical current density in $YBa_2Cu_3O_{7-\delta}$ films with nano-inclusions, PhD Thesis, University of Birmingham, United Kingdom: University of Birmingham.

[12] J. Feighan, A. Kursumovic, J. MacManus-Driscoll (2017), *Superconductor Science and Technology* **30**, 123001.

[13] M. Murakami, M. Morita, K. Doi, K. Miyamoto (1989), *Japanese Journal of Applied Physics* **28**, 1189.

[14] I. Nedkov, A. Veneva (1994), *Journal of Applied Physics* **75**, 6726.

[15] M.M. Dihom, A.H. Shaari, H. Baqiah, C.S. Kien, R.S. Azis, R. Abd-Shukor, N.M. Al-Hada, M.M.A. Kechik, Z.A. Talib (2019), *Journal of Superconductivity and Novel Magnetism* **32**, 1875.

[16] N. Mohd Hapipi, A.H. Shaari, M.M.A. Kechik, K.B. Tan, R. Abd-Shukor, N.R. Mohd Suib, S.K. Chen (2017), *Solid State Phenomena* **268**, 305.

[17] O. Ozturk, R. Arebat, A. Nefrow, F. Bulut, G. Guducu, E. Asikuzun, S. Celik (2019), *Journal of Materials Science: Materials in Electronics* **30**, 7400.

[18] N.A.M. Yamin, M.H.M. Zaid, K.A. Matori, J.L.Y. Chyi, S.N.F. Zalamin, N.A.N. Ismail, K.F. Chan, N. Effendy (2022), *Applied Physics A* **128**, 93.

[19] N.N. Mohd Yusuf, M.M. Awang Kechik, H. Baqiah, C. Soo Kien, L. Kean Pah, A.H. Shaari, W.N.W. Wan Jusoh, A. Sukor, S. Izzati, M. Mousa Dihom (2019), *Materials* **12**, 92.

[20] A. Ramli, A.H. Shaari, H. Baqiah, C.S. Kean, M.M.A. Kechik, Z.A. Talib (2016), *Journal of Rare Earths* **34**, 895.
[21] A. Bahboh, A.H. Shaari, H. Baqiah, C.S. Kien, M.M.A. Kechik, M.H. Wahid, R. Abd-Shukor, Z.A. Talib (2019), *Ceramics International* **45**, 13732.
[22] E. Nazarova, A. Zaleski, A. Zahariev, A. Stoyanova-Ivanova, K. Zalamova (2004), *Physica C: Superconductivity* **403**, 283.
[23] A.H. Salama, M. El-Hofy, Y.S. Rammah, M. Elkhatib (2015), *Advances in Natural Sciences: Nanoscience and Nanotechnology* **6**, 045013.
[24] P. Benzi, E. Bottizzo, N. Rizzi (2004), *Journal of Crystal Growth* **269**, 625.
[25] T.G. Holesinger, L. Civale, B. Maiorov, D.M. Feldmann, J.Y. Coulter, D.J. Miller, V.A. Maroni, Z. Chen, D.C. Larbalestier, R. Feenstra, X. Li, Y. Huang, T. Kodenkandath, W. Zhang, M.W. Rupich, A.P. Malozemoff (2008), *Advanced Materials* **20**, 391.
[26] R. Mohan, K. Singh, N. Kaur, S. Bhattacharya, M. Dixit, N.K. Gaur, V. Shelke, S.K. Gupta, R.K. Singh (2007), *Solid State Communications* **141**, 605.
[27] E. Hannachi, Y. Slimani, A. Ekicibil, A. Manikandan, F.B. Azzouz (2019), *Materials Chemistry and Physics* **235**, 121721.
[28] I. Hamadneh, A.M. Rosli, R. Abd-Shukor, N.R.M. Suib, S.Y. Yahya (2008), *Journal of Physics: Conference Series* **97**, 012063.
[29] A. Sedky, B. Abu-Ziad (2010), *Physica C: Superconductivity and its Applications* **470**, 659.
[30] A. Sedky (2009), *Journal of Physics and Chemistry of Solids* 70, 483.
[31] M.A. Almessiere, E. Hannachi, Y. Slimani, G. Yasin, M. Mumtaz, M.R. Koblischka, A. Koblischka-Veneva, A. Manikandan, A. Baykal (2020), *Materials Chemistry and Physics* **243**, 122665.